Parallel CFD International Conference (ParCFD2021)
May 17-19, 2021 (Online Conference)

Characterization of the pressure fluctuations within an airfoil boundary layer using WMLES

R. Boukharfane[§*], M. Parsani[*] L. Joly[‡] J. bodart[‡]

[*] King Abdullah University of Science and Technology (KAUST), ECRC, Thuwal, KSA
[§] Mohammed VI Polytechnic University (UM6P), MSDA, Benguerir, Morocco
[‡] Institut supérieur de l'aéronautique et de l'espace (SUPAERO), DAEP, Toulouse, France

May 17-19, 2021

Overview

1. *Motivation & Purpose*
2. *Wall-model details*
3. *Numerical setup*
4. *Numerical results*
5. *Conclusion & Perspectives*

Motivation & Purpose

Airfoil Noise Mechanisms

- Wall-pressure and loading fluctuations induced by a turbulent vortical field on a given airfoil can be caused by several mechanisms :
  - ✓ Turbulence-interaction, noise Tip noise, Vortex shedding noise, Stall noise, Trailing-edge noise
- For modern aircraft with turbofan engines:
  - ✓ At takeoff jet noise (rear arc) and fan noise (rear arc) are dominant, on approach airframe noise and fan noise are dominant

Special Features of Aeroacoustics in transonic flows

- Sound radiation is often a by-product of the unsteady flow
- Within a complex unsteady compressible flow the definition of sound is not obvious (most classical models are developed for incompressible flows)
- But adopting a mathematical definition of sound defines its sources
- Defining sources is not enough: radiation efficiency depends on much more...
- Modelling challenges
  - ✓ Flow physics, noise sources, numerical and HPC
- Spectrum of pressure, the convection velocity and the spanwise correlation length scale of the surface pressure fluctuations

Scope of the present study

- To carry out WRLES and WMLES simulations on simplified geometry (Controlled-Diffusion airfoil) relevant to CROR/UHBR fan trailing edge noise.
- To extract relevant quantities for current TE noise models from large-eddy simulations.
- To compare experimental results and LES.

Figure: Two dimensional cut of the Controlled-Diffusion airfoil

	Leading edge camber angle	Trailing edge camber angle	Thickness-to-chord ratio (max.)
CD airfoil	12°	12°	4.5%

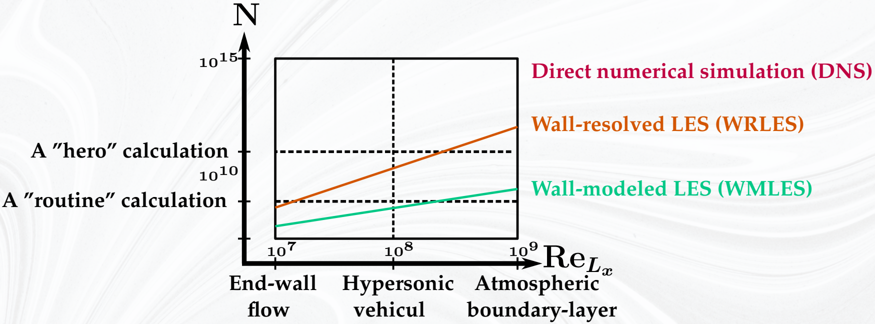

For the foreseeeable future, WMLES is the viable path to scale-resolvng simulations††.

†† Bose, S. T. & Park, G. I.
Wall-modeled large-eddy simulation for complex turbulent flows
Annual review of fluid mechanics (2018).

Wall-modeling methodology

- RANS-based wall model

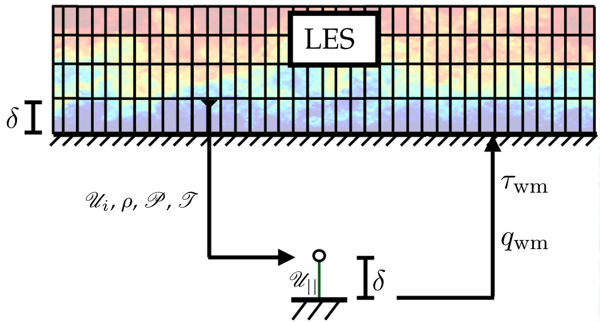

- ODE equilibrium wall-models

$$\frac{\partial}{\partial x_2}\left[\left(\mu+\mu_{t,\rm wm}\right)\frac{\partial \mathscr{U}_{||}}{\partial x_2}\right]=0,\quad \frac{\partial}{\partial x_2}\left[c_{\mathscr{P}}\left(\frac{\mu}{\rm Pr}+\frac{\mu_{t,\rm wm}}{{\rm Pr}_{t,\rm wm}}\right)\frac{\partial \mathscr{T}}{\partial x_2}\right]=-\frac{\partial}{\partial x_2}\left[\left(\mu+\mu_{t,\rm wm}\right)\mathscr{U}\frac{\partial \mathscr{U}_{||}}{\partial x_2}\right]$$

$$\mu_{t,\rm wm}=\kappa\sqrt{\rho|\tau_w|}\,x_2\left[1-\exp\left(-\frac{x_2^+}{A^+}\right)\right]^2,\quad \kappa=0.41,\quad A^+=17,\quad {\rm Pr}_{t,\rm wm}=0.9$$

Matrix of computations for WMLES assessment

- Focus the numerical simulations on 3 specific operating points.

	case	Ma_∞	Re	AoA	L_{x3}	N_{cells}	type of LES
$\mathscr{C}_1$	$\mathscr{C}_{1,\mathfrak{c}_1}$	0.3	8.30×10^5	$4°$	$10\%\ c$	225.1M	WRLES
	$\mathscr{C}_{1,\mathfrak{c}_2}$	0.3	8.30×10^5	$4°$	$10\%\ c$	19.9M	WMLES
	$\mathscr{C}_{1,\mathfrak{c}_3}$	0.3	8.30×10^5	$4°$	$10\%\ c$	19.9M	WRLES
$\mathscr{C}_2$	$\mathscr{C}_{2,\mathfrak{c}_1}$	0.5	2.29×10^6	$4°$	$10\%\ c$	225.5M	WRLES
	$\mathscr{C}_{2,\mathfrak{c}_2}$	0.5	2.29×10^6	$4°$	$10\%\ c$	19.9M	WMLES
	$\mathscr{C}_{2,\mathfrak{c}_3}$	0.5	2.29×10^6	$4°$	$10\%\ c$	19.9M	WRLES
$\mathscr{C}_3$	$\mathscr{C}_{3,\mathfrak{c}_1}$	0.5	2.29×10^6	$5°$	$20\%\ c$	451.0M	WRLES
	$\mathscr{C}_{3,\mathfrak{c}_2}$	0.5	2.29×10^6	$5°$	$10\%\ c$	19.9M	WMLES
	$\mathscr{C}_{3,\mathfrak{c}_3}$	0.5	2.29×10^6	$5°$	$10\%\ c$	19.9M	WRLES

Required amount of CPU time

More than 10 million h_{CPU} have been used thanks to the resources of the Supercomputing Laboratory (Shaheen) at KAUST in KSA and BSC at Barcelona in Spain.

Numerical solver : IC^3

- High-fidelity unstructured compressible flow solver for LES
- It solves the spatially-filtered compressible Navier-Stokes equations, using a finite volume formulation, control-volume based discretization on unstructured meshes.
- Numerical scheme non dissipative on perfectly regular grids, hybrid centered/upwind on low quality cells for stability
- Selectable Runge-Kutta (RK3, RK4) explicit time advancement
- highly scalable: IC^3 still fully exploit CPU based architectures with as low as 3000 grid points per CPU core

Flux discretization in IC^3

$$\mathfrak{F} = \frac{1}{V}\int_{\partial V} \mathbf{F}(\mathbf{q}) \cdot d\mathbf{S} = \sum_f (1 - f_{\alpha f})\mathfrak{F}_{\text{CENTRAL}} + f_{\alpha f}\mathfrak{F}_{\text{HLLC}}$$

Numerical details

- Vreman SGS model for the sub-grid terms.
- Unstructured control volume with a structured-like layer around the airfoil and unstructured elements in the far-field are used to reduce the computation cost.

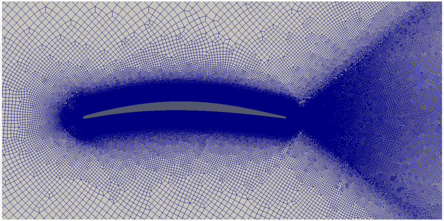

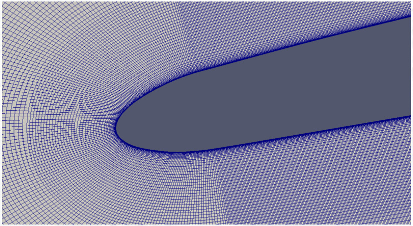

- Extrusion in the spanwise direction with a uniform cell size over a length L_{x_3}.

$$L_{x_3} \geq 2\delta_{\max}$$

Grid resolutions

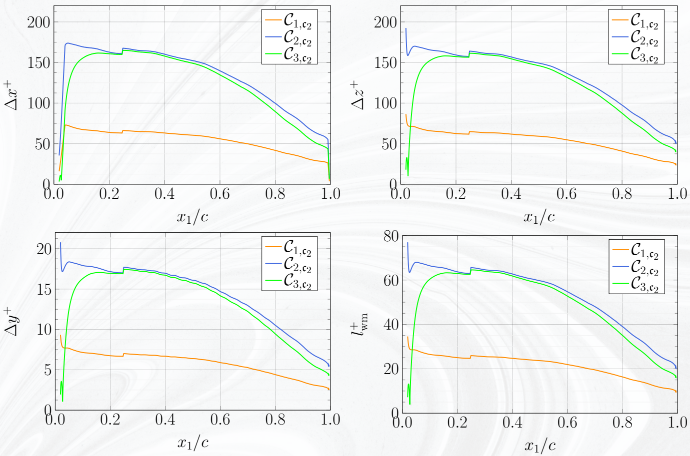

- WMLES simulations have $\Delta x_1 \approx \Delta x_3$.
- Δy^+ is less than 20 for WMLES
- 5 grid points off the wall in the LES mesh are matched to the wall–model top BL

Flow topolgy

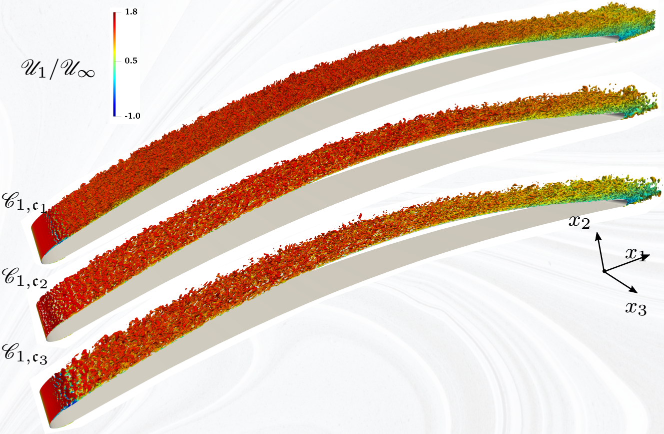

Topology of the flow described by the Q–criterion ($Q\,c^2 / \mathscr{U}_\infty^2 \sim 950$) and colored by the normalized longitudinal instantaneous velocity $\mathscr{U}_1 / \mathscr{U}_\infty$ for the $\mathscr{C}_1$ cases for which $\mathrm{Ma}_\infty = 0.3, \mathrm{Re} = 8.30 \times 10^5$ and $AoA = 4$.

- ✓ A laminar boundary-layer is present on the lower side of the airfoil, and a transitional and turbulent boundary layer on the upper side.
- ✓ WMLES cannot capture the leading edge bubble properly

Recirculation zone

(a) $\mathscr{C}_{1,\mathfrak{c}_1}$

(b) $\mathscr{C}_{2,\mathfrak{c}_1}$

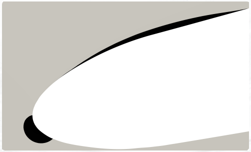

(c) $\mathscr{C}_{3,\mathfrak{c}_1}$

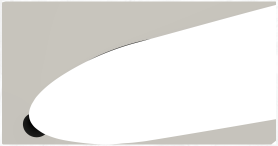

(d) $\mathscr{C}_{1,\mathfrak{c}_2}$

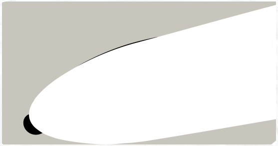

(e) $\mathscr{C}_{2,\mathfrak{c}_2}$

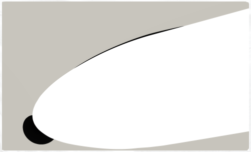

(f) $\mathscr{C}_{3,\mathfrak{c}_2}$

Visualization of the mean flow velocity sign for WRLES cases (top row) and WMLES cases (borrom row). Negative regions in black highlight the leading edge bubble.

Mean flow profiles

- Comparison of the time-averaged pressure coefficient distribution $C_{\mathscr{P}} = \frac{\langle \mathscr{P} \rangle - \mathscr{P}_\infty}{\frac{1}{2}\rho_\infty \mathscr{U}_\infty^2}$

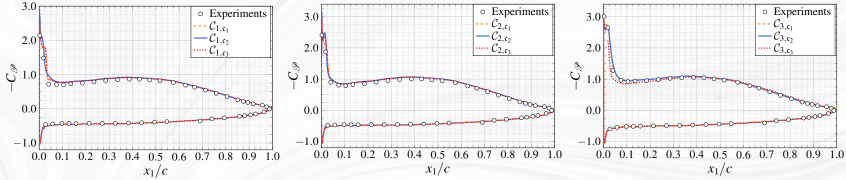

(a) $\mathscr{C}_1$ (b) $\mathscr{C}_2$ (c) $\mathscr{C}_3$

- Mean velocity normal to wall $\mathscr{U}_\perp$

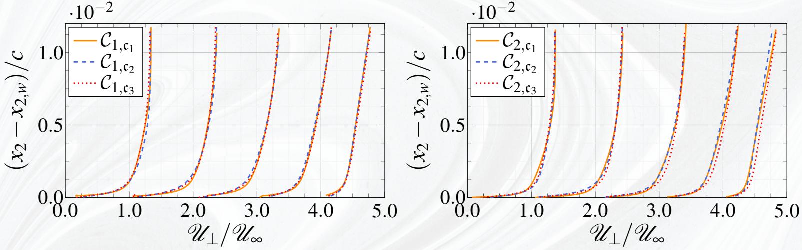

(a) (b)

Mean flow profiles

- Reynolds stress component

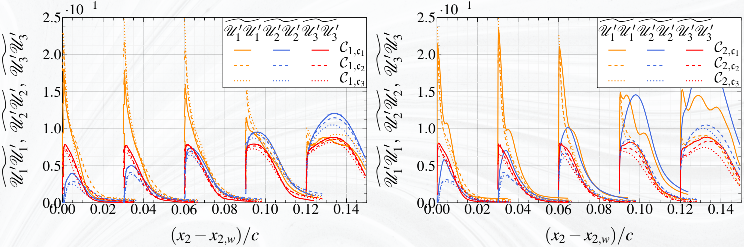

Resolved Reynolds shear stress profiles as a function of wall–normal distance at $x_1/c = 0.1$, 0.3, 0.5, 0.7 and 0.9. Each plot is separated by a horizontal offset of 0.03

- WMLES captures the trend followed by all the stress components.
- Underprediction of the magnitudes.

Frequency spectra of surface pressure fluctuations

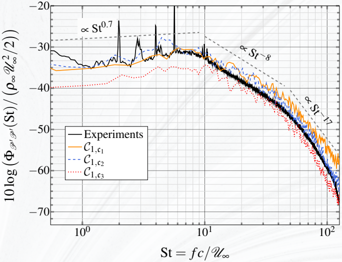

(a) $\mathscr{C}_1$

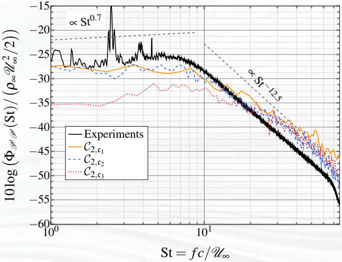

(b) $\mathscr{C}_2$

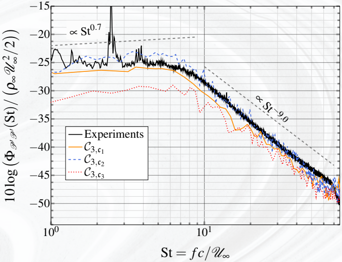

(c) $\mathscr{C}_3$

Wall pressure power spectral density (pressure side) at $x_1/c = 0.976$.

Convection velocity

The convection velocity is estimated as

$$\frac{\mathscr{U}_c(\xi_1)}{\mathscr{U}_{\text{edge}}} = \frac{\xi_1/\delta^\star}{\left[\tau \mathscr{U}_{\text{edge}}/\delta^\star\right]_{\max}},$$

where $\left[\tau \mathscr{U}_{\text{edge}}/\delta^\star\right]_{\max}$ represents the time lag.

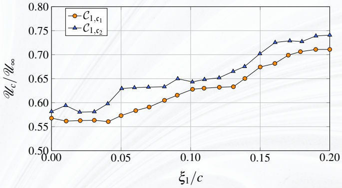

(a) $\mathscr{C}_1$

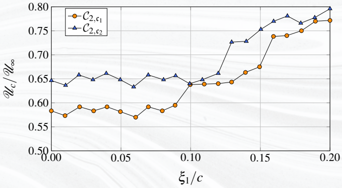

(b) $\mathscr{C}_2$

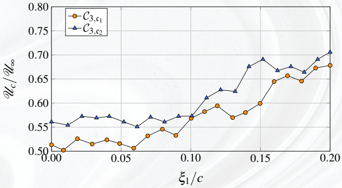

(c) $\mathscr{C}_3$

Reference probes used for the longitudinal spacing ξ_1 is $x_{\text{ref}} = 0.978$

Spanwise coherence length

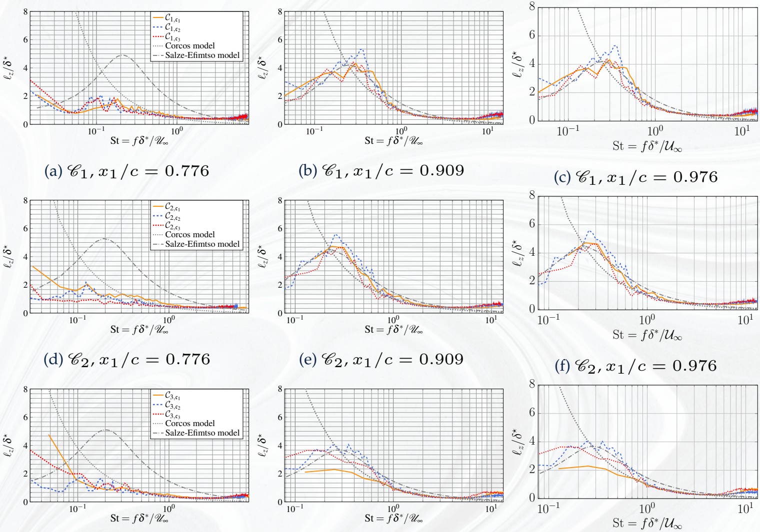

(a) $\mathscr{C}_1, x_1/c = 0.776$ (b) $\mathscr{C}_1, x_1/c = 0.909$ (c) $\mathscr{C}_1, x_1/c = 0.976$

(d) $\mathscr{C}_2, x_1/c = 0.776$ (e) $\mathscr{C}_2, x_1/c = 0.909$ (f) $\mathscr{C}_2, x_1/c = 0.976$

(g) $\mathscr{C}_3, x_1/c = 0.776$ (h) $\mathscr{C}_3, x_1/c = 0.909$ (i) $\mathscr{C}_3, x_1/c = 0.976$

Spanwise coherence length at different locations close to the trailing edge for the three cases.

Conclusion & Perspectives

Conclusion

- Very good matching with experiments despite:
- Confidence in the predictions in the region of interest (TE)
- "Large" physical time required to reach convergence in the high order statistics
- Even at transonic Mach numbers, the predicted coherence length is close to the Salze model
- Reduction of the computational cost of WMLES by 2 orders of magnitude compared to that of classic WRLES
  - ✓ Reducing the number of grid points by roughly $\sim 1/20$
  - ✓ Increasing the time step by more than one order of magnitude because the grid for the WRLES is much less constrained by the acoustic time-step limitation.

Perspectives

- Perform 3D blades
- Sliding mesh computations of a single rotating blade using wall-modelling

Thanks for tuning in!
Please leave comments & questions

Acknowledgments

Barcelona Supercomputing Center
Centro Nacional de Supercomputación